

Air Ducted Blade Design for Horizontal Axis Wind Turbines

Cemil Yigit (✉ cyigit@sakarya.edu.tr)

Original article

Keywords: Horizontal axis wind turbine, Blade design, Response surface optimization method, Computational fluid dynamics, Power coefficient

Posted Date: February 18th, 2020

DOI: <https://doi.org/10.21203/rs.2.23863/v1>

License:  This work is licensed under a Creative Commons Attribution 4.0 International License.

[Read Full License](#)

Air Ducted Blade Design for Horizontal Axis Wind Turbines

Cemil Yigit

Mechanical Engineering Department, Engineering Faculty, Sakarya University, Serdivan, Sakarya 54187, Turkey

Correspondence: cyigit@sakarya.edu.tr

Abstract

Background: Medium and small-scale wind turbines with no pitch control are cheaper than their controlled equivalents but are much more affected by aerodynamic stall, and local boundary layer separation occurs on the blade when critical wind speed is exceeded. As a result, they produce relatively low power. In this study, the delay of separation of the boundary layer from the surface was investigated by increasing the kinetic energy of the low-momentum fluid behind the surface utilizing the airflow from the air ducts added on the blade.

Methods: To obtain the optimum performance from the blade, a computer-aided optimization study was conducted by taking the slope, diameter, number, and angle of attack parameters of the air ducts. The response surface methodology, a goal-oriented and multi-purpose method, was used as an optimization method to provide the best possible design according to the constraints and targets set for the parameters.

Results: Optimum parameter values were determined using computational fluid dynamics analysis, and air ducted blade design was compared with the air duct-free blade design, and as a result, the power coefficient obtained from the blade was improved between 3.4% and 4.4% depending on wind speed.

Conclusions: Opening air ducts up to a critical number of ducts increase viscous forces. This provides more power from the rotor. On the other hand, with the extra airflow coming from the air ducts, the flow separation behind the wing is delayed and the stall effect is shifted to higher wind speeds and the rotor can work for a longer time at nominal power. Besides, since all this is done with passive flow control, a remarkable increase in annual electricity production from the turbine is provided.

Keywords: Horizontal axis wind turbine, Blade design, Response surface optimization method, Computational fluid dynamics, Power coefficient.

Background

Because of the limited amounts of fossil fuels and their negative impact on the environment, the search for renewable and clean energy sources has been going on for a long time, especially to generate electricity. Wind energy is one of these renewable and clean energy sources, perhaps one of the most important. However, the effective use of these resources is directly related not only to the improvement of financing opportunities, infrastructure or legislation related to renewable energy sources and electricity generation but also to the improvement of the efficiency of the processes in which electricity generation is carried out [1, 2].

From this point of view, the turbine blade is one of the basic building elements that make up the

wind turbine power plant; Since it is the main equipment where the kinetic energy of the air is transformed into mechanical energy, improving its performance directly increases the efficiency of the wind power plant. When the literature was examined, it was observed that the studies were generally focused on the framework of improving the performance and optimum use of the main equipment that makes up the wind power plant to increase the annual electricity energy generated from the plant. Many researchers have proposed new blade profiles and new blade designs using these profiles to improve horizontal axis wind turbine (HAWT) performance. Maalawi and Badawy [3] attempted to improve blade performance by analytically determining the optimal beam width and angle of rotation, Xudong

et al. [4], in addition to these parameters, tried to obtain the most appropriate blade design to achieve maximum performance by taking into account the beam thickness. In addition to the studies [5, 6] examining the effects of different blade types on performance, some researchers [7-9] have developed numerical code based on the blade element momentum theory (BEM), while others [10, 11] have been able to develop a packaged software for blade design that gives the best performance, taking into account many parameters such as the dynamic and mechanical properties of the material from the phase of the turbine blade sizing to the production phase. Some researchers [12, 13] tried to improve blade performance by making systematic changes to the blade profile. Doquette and Visser [14] examined the effects of the number of blades and the tilt of the blade on turbine efficiency, and it was found that the power coefficient increased, especially in small-scale wind turbines, depending on the number of blades. Several studies have been also carried out to improve the performance of small-scale wind turbines at low speeds [15-18], the effects of the flexibility and stiffness of blades on deformation and performance under different wind speeds have been investigated.

Active and passive flow control to improve wind turbine performance has long been the focus of researchers' attention. Flow control can be performed to delay or bring forward the transition from the laminar flow and to increase or suppress turbulence, and as a result, friction and lifting forces are tried to be reduced or increased in line with the targets. At high speeds, flow separation caused by curvature on the blade surface can be delayed by flow mixtures within the boundary layer. Studies are carried out on active control systems providing continuous and pulsed air jets, where flow separation is delayed by re-energizing the boundary layer by various means, and on passive control systems such as swirl vane blades, shape optimizations and roughness elements [19-26]. Especially by using roughness elements, studies that delayed turbulence and flow separation have been carried out on aircraft wings for many years. It was determined that the studies in the literature made modifications to increase

performance such as shape optimization, roughness element and fin usage on the blade profile, in addition to this, the optimization of the number of blades, dimensions, position, and composite material were carried out.

To combat global warming and climate change sustainably and effectively, it is extremely important to reduce greenhouse gas emissions that are released during the combustion of fossil fuels radiating to the atmosphere in the electricity generation process. One way is to make power plants, such as wind turbines, that generate electricity using alternative energy sources more preferable.

Especially medium and small-scale wind turbines without pitch control are cheaper than their controlled equivalents, but they are much more affected by aerodynamic stall, and local boundary layer separation occurs on the blade when critical wind speed is exceeded. Unlike the literature, in this study flow separation is delayed and wind turbine blade performance is increased by using passive flow control. Thus, the turbine was operated longer under the high-power coefficient. For this purpose, the kinetic energy of the low momentum airflow in the area close to the surface behind the blade is increased by using air ducts that are added to the blade of the wind turbine and the separation of the boundary layer from the surface is delayed. Thus, the power coefficient value obtained from the blade is improved.

Methods

Studies on active control systems that provide continuous and pulsed air jets and passive control systems such as swirl-producing fins and roughness elements, where flow separation is delayed by re-energizing the boundary layer, can be carried out. Utilizing a series of air ducts that will be designed on the blade according to the local velocity vector, the kinetic energy of the low-momentum fluid close to the surface can be increased by providing the interaction between the airflow on the surface and the air jet coming out of the ducts.

The forces that are effective on the wind turbine blade are pressure and wall shear stress, their flow-

direction components form drag (F_D) forces, while components perpendicular to the flow form lifting (F_L) forces. Differential drag and lifting force on the dA surface in two-dimensional flow can be written as in Eq. (1) and (2), respectively [27].

$$F_D = \int_A (-P \cdot \cos \theta + \tau_w \sin \theta) dA \quad (1)$$

$$F_L = \int_A (-P \cdot \sin \theta - \tau_w \cos \theta) dA \quad (2)$$

As can be seen from the equations, both drag and lifting force is influenced by the wall shear force and pressure forces on the blade surface. The wall shear force depends on the shape of the blade, the length of the boundary layer and the wall shear stress, while the pressure force depends on the front view area of the blade and the pressure difference between the surfaces. Since different parameters are effective on these two forces, it is inevitable that the pressure force decreases or vice versa when increasing the wall shear force.

Air ducts were opened on the blade, the boundary layer was extended, so the wall shear force was increased, therefore, as the front view area of the blade was reduced to the total duct area, some reduction in the pressure force value would occur. In addition to the pressure drop caused by friction losses as the length of the duct is short, the pressure drop resulting from local losses in the duct inlet and outlet will be small due to low fluid density and flow rates ($\Delta P \approx 0.75\rho V^2$), therefore, when the pressure force value to be lost in surface forces by opening ducts is compared to the viscous forces value to be increased by extending the boundary layer, it is expected that the opening of the air ducts will have a positive effect on drag and lifting forces, especially at low speeds. For these reasons, it is aimed in the study to make maximum the sum of wall shear force and pressure force and parameter levels in which flow separation will be delayed.

A computer-aided numerical optimization method was used to save both time and costs during the study of blade performance. Response Surface Optimization (RSO) Methodology is a widely used mathematical and statistical method for modeling and analyzing a process in which a

parameter intended to be optimized is affected by several variables [28, 29]. The diameter, slope, and the number of the air duct, which was opened in the region close to the root section on the blade, and the angle of attack of the blade were taken as parameters. After the upper and lower limits that each parameter can take were determined separately, critical values for the parameters that will make the power coefficient maximum were found by computer-aided optimization method. For this purpose, the turbine blade with air ducts was created (Fig. 1).

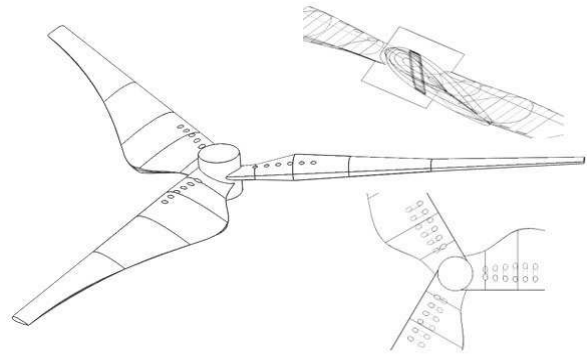


Fig. 1 Horizontal-axis wind turbine with duct

Wind speed is influenced by many factors such as climate change as well as natural and artificial geographic buildings, and although these effects vary year-on-year, also they provide information about average wind speeds in various regions around the world as a result of measurements and analyses conducted within the scope of scientific research. Cortesi et al. [30] conducted a study of wind speed characteristics in Europe, depending on weather conditions, and found that the average annual wind speed varies between 7-10 m/s in regions with high wind speeds such as northern Scandinavia, southern Spain, and the Aegean Sea. Hasager et al. [31] used satellite (Satellite SAR, Synthetic Aperture Radar) images to determine wind characteristics on the high seas, and found the average wind speed in the southern parts of the North Sea as 7 m/s. On the other hand, when the MERRA (Modern-Era Retrospective Analysis for Research and Application) and Global CFDDA (Climate Four-Dimensional Data Assimilation) reanalysis datasets published by Global Wind Atlas were examined, it was determined that the widespread wind speed in the world ranged from

6 m/s to 7 m/s. To provide a widespread impact, the optimization study was carried out in the wind speed range of 6-8 m/s [32].

Numerical Study

The 3D calculation zone was created using ANSYS/Design Modeller software. It is important that the calculation zone is created as large as possible so that the results of the analysis are not affected by the limits of the calculation zone. However, it should be taken into consideration that this situation will increase the number of elements in the mesh structure of the model and the time of analysis. The calculation zone has a cylindrical shape and can be defined periodically for each blade. Therefore, a computational region was defined in which a single blade was located. On the other hand, considering that the Mach value in the analyses was very small (0.018-0.023), the size independence study was performed, and the limits of the calculation area were determined depending on the rotor diameter (Fig. 2).

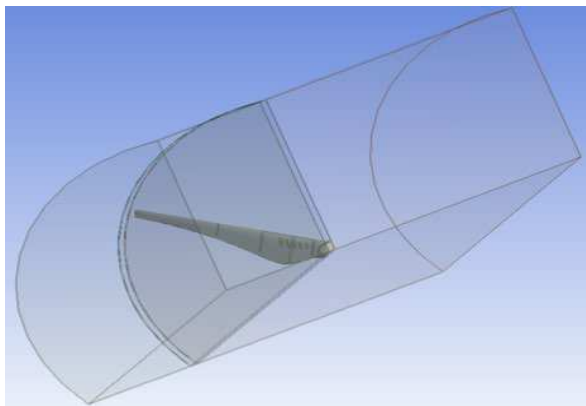


Fig. 2 3D periodic calculation zone and boundary conditions

In practice, the calculation zone can be taken 10 times the diameter to ensure that the flow is fully developed when it comes to the blades, but this will greatly increase the calculation zone and, as it is, the number of elements in the analysis. Therefore, a parabolic speed entry limit requirement was defined to the model using UDF (user-defined function), and 2 times the diameter was left from the entrance up to the blade. The length of the calculation zone will be taken 6 times

the diameter so that the turbine back-flow part is not affected by the exit limit condition.

For computational fluid dynamics (CFD) analyses, a triangular pyramid mesh structure containing tetrahedron elements was preferred. The mesh structure must be proper in terms of the accuracy of the results. Therefore, it was sensitive to keeping the skewness values of the mesh to be created within the desired limits ($0.50 \leq \text{skewness} \leq 0.80$). On the other hand, the areas close to the blade surface where relatively precise calculations were needed, and the mesh structure around the ducts were composed of smaller elements than other regions by using a weight factor. Figure 3 shows the mesh structure used in CFD analysis.

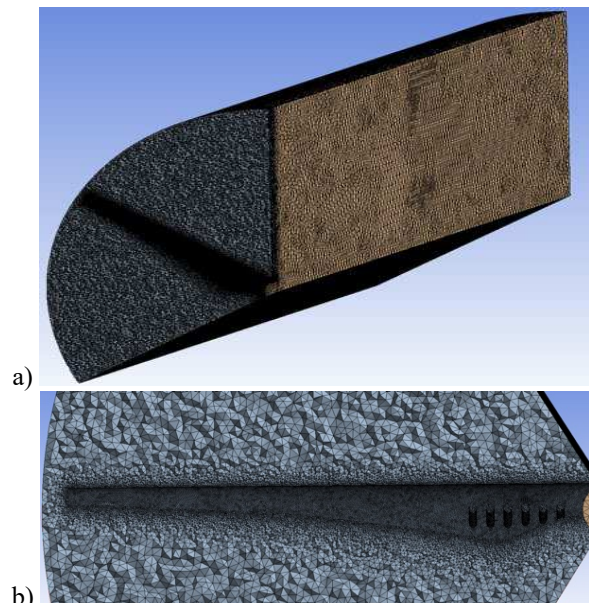


Fig. 3 a) The mesh structure of the 3 model, b) The mesh structure around of the blade

The maximum, minimum and average skewness values of the mesh structure that make up the calculation zone were 0.948, 4.405×10^{-6} and 0.236, respectively. It can be said that the mesh structure is appropriate because the maximum skewness value of the mesh is below the maximum skewness value accepted in the literature (0.98) [33]. On the other hand, the mesh structure contains 1113020 nodes and 6054957 elements, also after approximately 6 million elements, it is seen that increasing the number of elements has no significant effect on the results, so the analysis is independent of the mesh structure.

The pressure-based time-dependent formulation was used in analyses by using ANSYS/Fluent software. As a turbulence model, k-epsilon RNG with a result of less than 5% error was preferred in horizontal-axis wind turbines [34]. In the turbulence model, y^+ is preferred to be around 1 for an effective solution [33]. However, for the average grid ($1 < y^+ < 30$) range, the turbulence model provides consistent wall shear stress values. Although the model does not reach y^+ value of around 1, it varies around the average grid range ($4 < y^+ < 7$). Reducing y^+ to 1 for the prepared model brings a serious processor and RAM load to the analysis.

The calculation zone was defined in atmospheric conditions. The mesh motion method, which allows angular velocity to be given to the blade and rotor, was used and, angular velocity was not given to the flow volume surrounding the blades. The time step (ΔT) was defined as the function of blade speed, length, and tip speed ratio. The mean moment coefficient ($C_{m,avg}$) was used when calculating torque and power accordingly. The moment coefficient values of the turbine were monitored depending on the time until the turbine makes 10 cycles and the average moment coefficient was calculated from these data. The average torque (T_{avg}) was calculated depending on airspeed and density, mean moment coefficient, turbine projection area, and chord (c) length. The power coefficient (C_p) was calculated as a function of torque data from the numerical model and angular velocity and the power of air coming into the turbine.

Within the scope of numerical calculations, flow velocity and pressure fields were obtained, and momentum, stability and pressure correction equations were solved respectively. After the model was first solved with a numerical analysis method used for solving first-degree finite volumes, the first solution was introduced as the initial condition to the model and the results were obtained with a numerical analysis method used for solving second-degree finite volumes. To determine the convergence of analysis, not only the values obtained from the velocity field updated with the equations were not compared to the

values obtained from the previous iteration, but also the variation of dimensionless numbers, highly effective on the aerodynamic characteristic of the blade such as lift and moment coefficient, was followed throughout iterations. It was decided that the values obtained from the speed field provided convergence criteria (>0.001) and that analyses made convergence under conditions where the dimensionless numbers that were followed were no longer changed by iterations. Verification experiments were conducted to prove the reliability of the results obtained from analyses.

Validation

Within the scope of analyses, the angle of attack of the blade, the diameter, inclination, and number of the air duct were taken as parameter to determine the best blade design to give high performance to the wind turbine made of composite material (Epoxy-glass) with a blade length of 1.24 m, a rotor diameter of 2.6 m and a sweeping area of 5.31m², at wind speed of 6-8 m/s. To determine the reliability of the results obtained from analyses, validation experiments were conducted for wind turbines air ducted and duct-free blades. The average power coefficient ($C_{p,avg}$) obtained from the wind turbine depending on the electrical and wind power was defined in Eq. (3).

$$C_{p,avg} = \frac{\int_0^{2\pi} \frac{P_{e,\theta}}{P_{\infty}\eta_g} d\theta}{n} \quad (3)$$

where θ is the angular position of the wind turbine, $P_{e,\theta}$ is the electrical power generated by the generator depending on the angular position, P_{∞} is wind power, n is the number of time steps in which the turbine returns to complete around, and η_g is the generator efficiency. Mechanical losses were neglected as the moment was transferred directly to the generator with a short shaft without using any gear system. Uncertainty analysis was performed for measurements carried out within the scope of the experimental study. When determining the power coefficient, the error rate was determined as $\pm 2.2\%$ using the Eq. (4) depending on the measurements of flow (I;

0.2%+4d, Brymen BM525s), voltage (V; 0.08%+2d, Brymen BM525s) and wind speed ($\pm 2\% + 0.2\text{m/s}$, Lutron AM-4206). Furthermore, while the blade tip velocity rate was determined, the error rate encountered based on wind speed and angular velocity ($\pm 0.04\% + 2$, UNI-T UT 372) measurements were found as $\pm 3.6\%$ by using Eq. (5).

$$\sigma_P = \sqrt{\left(\frac{\partial P}{\partial I} \sigma_I\right)^2 + \left(\frac{\partial P}{\partial V} \sigma_V\right)^2 + \left(\frac{\partial P}{\partial u} \sigma_u\right)^2} \quad (4)$$

$$\sigma_\lambda = \sqrt{\left(\frac{\partial \lambda}{\partial \omega} \sigma_\omega\right)^2 + \left(\frac{\partial \lambda}{\partial u} \sigma_u\right)^2} \quad (5)$$

A comparison of the power coefficient values obtained from experimental studies and CFD analyses is shown in Figure 4. The average value obtained from the experiments for each tip-speed ratio is shown in the graph. It is observed that curves formed for the experimental data are compatible with the CFD results. The results showed a 5.3% error in low blade tip speed rates, while increased by up to 6.8% in high tip speed rates.

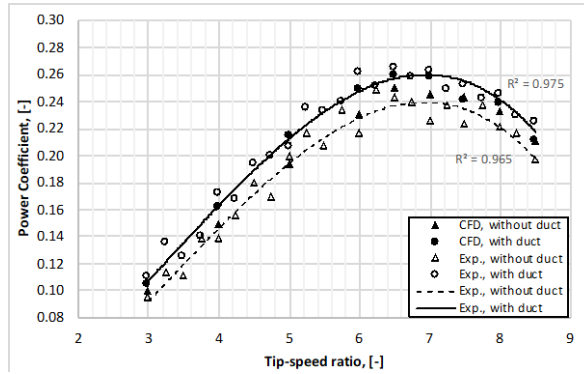


Fig. 4 Comparison of the experimental study and CFD analysis results performed at 6 m/s air velocity and 7 tip-speed ratio

Results and discussion

Within the scope of the optimization study for air ducted blade design, the shape parameters to maximize the power that can be obtained from the blade and the maximum and minimum range of values these parameters can receive were defined in ANSYS/Response Surface Optimization software. Thus, taking into account the constraints defined according to the shape parameters, the air

ducted blade design capable of giving maximum power was realized. The effects of air ducts in the optimized new blade design on performance improvement were determined by comparing the air duct-free blade.

To compare the effect of air ducts, CFD analyses of air duct-free blade were performed at different attack angles. For the blade tip speed ratio of 7, the power coefficient values obtained depending on the angle of attack at different wind speeds ranging from 6 m/s to 8 m/s are shown in Figure 5. In the wind speed range, which is aimed to improve blade performance, relatively high-power coefficient values were obtained between 5° and 8° angles of attack for air duct-free blade design.

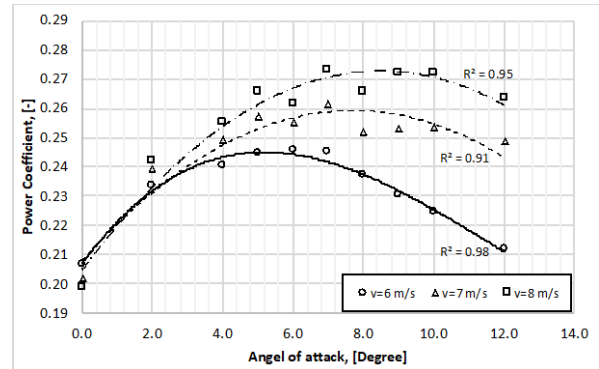


Fig. 5 Power coefficient values, based on the angle of attack at different airspeeds for air duct-free blade design

In the optimization study, the optimum parameter values for air ducted blade design at 7° angle of attack are 18 mm, 35° and 6, respectively, for duct diameter, tilt, and number. Figure 6 shows power coefficient values and maximum power curves based on various blade tip speed ratios from air ducted and duct-free blade designs at wind speeds of 6, 7 and 8 m/s. The stall effect on the tested blades depends on airspeed, but when the blade tip speed ratio exceeds approximately 7, it is seen. When the maximum power curves of air ducted and duct-free blade designs were examined, it was determined that the air ducts on the blade increased the power coefficient by 2.2-4.4%.

When the critical wind speed, which varies depending on the shape parameters of the blade, is exceeded, local boundary layer separations occur on the blade. Thus, the turbine produces low

power, especially at high wind speeds. With the air ducts on the blade, sufficient momentum is transferred to the boundary layer to prevent flow separation, and by increasing the kinetic energy of the low-momentum fluid in the area close to the surface, the boundary layer separation from the surface is delayed.

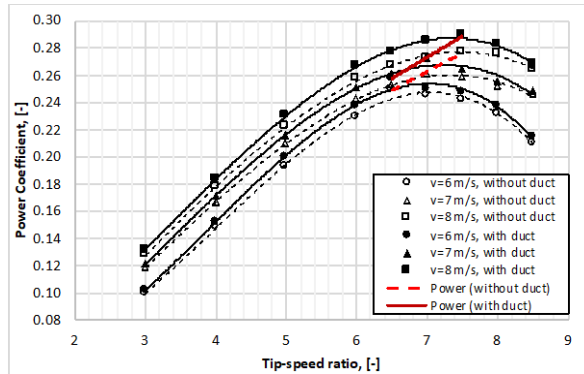


Fig. 6 Power coefficients and maximum power curves obtained from the blade, which is designed with and without air ducts at various wind speeds, depending on the blade tip speed ratio

Figure 7 shows flow lines and turbulence kinetic energy gradient in the blade profile section. In the air ducted blade design, the extra airflow from the ducts increases the kinetic energy of the low momentum airflow on upper surface of the blade profile, thereby delaying the separation of the flow (yellow mark). This allows the blade to run longer at the high-power coefficient. Under the same conditions, it appears that flow separation occurs on the upper surface of the blade profile (red mark), which does not have air ducts.

In Figure 8, the pressure differential values on the plane passing through the center of the air ducts are shown comparatively for air ducted and duct-free blade designs. The pressure difference in the first three ducts of the 6-duct blade design is greater than the duct-free blade profile, while from the 4th duct, the pressure difference value is higher in the duct-free blade profile. Considering that the pressure difference on the blade is directly related to the pressure forces and the torque value that can be obtained from the blade and that this change in torque will be greater in areas away from the root where the blade speed is relatively high, this situation indicates the existence of a critical number of ducts. Air ducts on the blade increase

the wall shear forces as well as significantly reducing pressure forces after a critical number of ducts. Also, after the critical number of ducts, the gain from the peripheral shift forces cannot supply the loss of pressure forces and the blade loses power. Therefore, determining the optimum number of air ducts is very important.

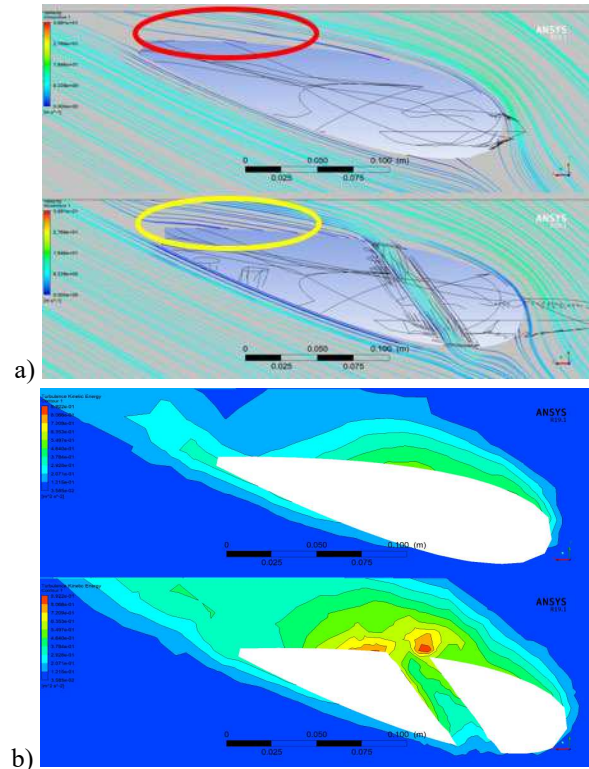


Fig. 7 a) Streamlines in the blade profile section, b) Turbulence kinetic energy in the blade profile section

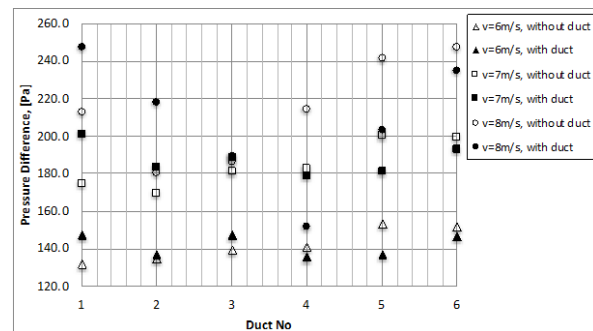


Fig. 8 Maximum pressure differences on the plane passing through the centre of the air ducts

Conclusions

To obtain maximum power from the air ducted blade design, the Response Surface Optimization method was used to determine the optimum values of parameters such as duct diameter, tilt, number and angle of attack of blade. Thus, a targeted optimization was made that provides the best

possible design according to the constraints and targets set for the optimization parameters.

Opening the air ducts on the blade increases the viscous forces while decreasing the pressure forces. In order to minimize the effect of the decrease in pressure forces, the air ducts are located in the max chord section which is near the root section of the blade. However, given that the total force on torque is effective, a critical number of channels must be defined. Because the increase in viscous forces after the number of critical channels cannot compensate for the decrease in pressure forces. Although the number of critical ducts varies depending on the shape parameters, angle of attack and wind speed, 6-ducted blade design has come into prominence in the 7° angle of attack in CFD analysis.

With the passive flow control method, a sufficient amount of momentum is transferred to the area where the air ducts are located, and the airflow is attached to the upper surface of the blade. Thus, the blade is provided to work longer with the maximum power coefficient.

According to the results obtained from CFD analysis, the air ducts added on the blade increased the power coefficient between 3.4% and 4.4% depending on the wind speed. Considering that the highest theoretically achievable aerodynamic efficiency of turbine blades, known as the Betz limit, is approximately 59% and that the medium-sized commercial horizontal-axis turbines operate at approximately 25-35% efficiency, this would be regarded as a significant increase.

According to the literature, rotor performance can be increased by active flow control such as pitch and yaw control. However, in this study, without an external energy input into the system, the performance was increased with passive flow control by utilizing air ducts. This provides a serious increase in the annual electricity production (AEP) of the wind turbine.

In addition to the development of the existing parameters, further studies will be carried out to reach higher power coefficient values by enriching the parameters of the air duct, such as using different duct shapes and reducing the diameter of the duct from the inlet to the exit. Thus, it is aimed to make the use of wind energy, which is a clean

and renewable energy source, for electricity generation more economically attractive in the future.

Abbreviations

AEP: Annual electricity production; BEM: blade element momentum; CFD: Computational fluid dynamics; CFDDA: Climate four-dimensional data assimilation; HAWT: horizontal axis wind turbine; MERRA: Modern-era retrospective analysis for research and application; RNG: Renormalization group; RSO: Response surface optimization; UDF: User defined function.

Nomenclatures

c	Chord, [m]
C_m	Moment coefficient, [-]
C_p	Power coefficient, [-]
F_D	Drag coefficient, [kgms ⁻²]
F_L	Lift coefficient, [kgms ⁻²]
I	Current, [ampere]
P	Pressure, [kgm ⁻¹ s ⁻²]
P_e	Electrical power, [kgm ² s ⁻³]
P_∞	Available (wind) power, [kgm ² s ⁻³]
T_{avg}	Average torque, [kgm ² s ⁻²]
u	Air velocity, [ms ⁻¹]
V	Voltage, [volt]
η_g	Generator efficiency, [-]
λ	Tip-speed ratio, [-]
σ_λ	Error in tip-speed ratio measurement, [-]
σ_P	Error in power measurement, [-]
τ_w	Shear stress, [kgm ⁻¹ s ⁻²]
ω	Angular velocity, [rads ⁻¹]

Declarations

Ethics approval and consent to participate

Not applicable

Consent for publication

Not applicable

Availability of data and materials

The datasets used and analyzed during the current study are available from the author on reasonable request.

Competing interests

The author declares that he has no competing interests.

Funding

Not applicable

Author's contributions

The author read and approved the final manuscript.

Acknowledgements

Not applicable

References

1. Saundry PD (2019) Review of the United States energy system in transition. *Energy, Sustainability and Society* 9(4):1-32
2. Raheem et al (2016) Renewable energy deployment to combat energy crisis in Pakistan. *Energy, Sustainability and Society* 6(16):1-13
3. Maalawi, KY, Badawy MTS (2001). A direct method for evaluating performance of horizontal axis wind turbines. *Renewable and Sustainable Energy Reviews* 5(2):175-190
4. Xudong X et al. (2009). Shape optimization of wind turbine blades. *Wind Energy* 12(8):781-803
5. Xu L, Xu L, Zhang L, Yang K (2015). Design of wind turbine blade with thick airfoils and flat back and its aerodynamic characteristic. *The Open Mechanical Engineering Journal* 9:910-915
6. Lee MH, Shiah YC, Bai CJ (2016). Experiments and numerical simulations of the rotor-blade performance for small-scale horizontal axis wind turbine. *Journal of Wind Engineering and Industrial Aerodynamics* 149(C):17-29
7. Lanzafame R, Messina M (2010). Power curve control in micro wind turbine design. *Energy* 35(2):556-561
8. Abolfazl P, Peyman ANA, Mehdi A, David W (2016) Aero-structural design and optimization of a small wind turbine blade. *Renewable Energy* 87(P2):837-848
9. Ashrafi ZN, Ghaderi M, Sedaghat A (2015) Parametric study on off-design aerodynamic performance of a horizontal axis wind turbine blade and proposed pitch control. *Energy Conversion and Management* 93:349-356
10. Jureczko M, Pawlak M, Mezyk A (2005) Optimization of wind turbine blades. *Journal of Materials Processing Technology* 167(2-3):463-471
11. Rehman S, Alam MdM, Alhems LM, Rafique MM (2018) Horizontal axis wind turbine blade design methodologies for efficiency enhancement. *Energies* 11(3):506-540
12. Mahdi NA, Farzad M, Mehdi S (2016) Performance improvement of a wind turbine blade using a developed inverse design method. *Energy Equipment and Systems* 4(1):1-10
13. Karthikeyan N, Kalidasa MK, Arun KS, Rajakumar S (2015) Review of aerodynamic developments on small horizontal axis wind turbine blade. *Renewable and Sustainable Energy Reviews* 42:801-822
14. Duquette MM, Visser KD (2003) Numerical implications of solidity and blade number on rotor performance of horizontal-axis wind turbine. *Journal of Solar Energy Engineering* 125(4):425-432
15. Ponta FL, Otero AD, Lago LI, Rajan A (2016) Effects of rotor deformation in wind-turbine performance: the dynamic rotor deformation blade element momentum model (DRD-BEM). *Renewable Energy* 92:157-170
16. Wang J, Qin D, Lim TC (2010) Dynamic analysis of horizontal axis wind turbine by thin-walled beam theory. *Journal of Sound and Vibration* 329(17):3565-3586
17. Tummala A et al. (2016) A review on small scale wind turbines. *Renewable and Sustainable Energy Reviews* 56(C): 1351-1371
18. Scappatici L et al. (2016) Optimizing the design of horizontal-axis small wind turbines: from the laboratory to market. *Journal of Wind Engineering and Industrial Aerodynamics* 154(C):58-68
19. Fatehi M et al. (2019) Aerodynamic performance improvement of wind turbine blade by cavity shape optimization. *Renewable Energy* 132:773-785
20. Seo S, Hong C (2016) Performance improvement of airfoils for wind blade with groove. *International Journal of Green Energy* 13(1):34-39

21. Liu H et al. (2017) A parametric investigation of endwall vortex generator jet on the secondary flow control for a high turning compressor cascade. *Journal of Thermal Science and Technology* 12(1):1-12
22. Sundaravadivel TA, Pillai SN, Kumar CS (2013) Influence of boundary layer control on wind turbine blade aerodynamic characteristic – Part I – Computational Study. In: 8th Asia-Pacific Conference on Wind Engineering (APCWE-VIII), December 10-14, Chenna, India, p. 1211-1217
23. Chishty MA, Hamdani HR, Parvez K (2013) Effect of turbulence intensities and passive flow control on LP turbine. In: 10th International Bhurban Conference on Applied Science&Technology (IBCAST), January 15-19, Islamabad, Pakistan
24. Fernandez-Gamiz U et al. (2017) Five-megawatt wind turbine power output improvements by passive flow control devices. *Energies* 10(6):742-757
25. El-Gendi MM, Ibrahim MK, Mori K, Nakamura Y (2010) Novel flow control method for vortex shedding of turbine blade. *Trans. Japan Soc. Aero. Space Sci.* 53(180):122-129
26. Seifert A, Stalnov O, Troshin V, Avnaim MH (2012) On the application of active flow control to wind turbines. *Fluids Engineering Division Summer Meeting*, p. 3057-3064 DOI: 10.1115/AJK2011-13006
27. Cengel YA, Cimbala JM (2013) *Fluid Mechanics: Fundamental and Applications*. McGraw-Hill Companies. New York
28. Braimah MN, Anozie AN, Odejebi OJ (2016) Utilization of response surface methodology (RSM) in the optimization of crude oil refinery process. *Journal of Multidisciplinary Engineering Science and Technology (JMES)* 3(3):4361-4369
29. Montgomery DC (2005) *Design and Analysis of Experiments: Response Surface Method and Designs*. John Wiley & Sons. New Jersey
30. Cortesi N et al. (2019) Characterization of European wind speed variability using weather regimes. *Climate Dynamics* 53(7-8):4961-4976
31. Hasager CB et al. (2015) Using satellite sar to characterize the wind flow around offshore wind farms. *Energies* 8:5413-5439
32. Global Wind Atlas (2019) Mean wind speed at 100 m above the surface. Available at <http://science.globalwindatlas.info/datasets.html>. Accessed 1 September 2019
33. Ansys (2019) *Fluent user guide*. Available at <https://support.ansys.com/AnsysCustomerPortal/>. Accessed on 8 October 2019
34. Yigit C (2018) Improving the horizontal axis wind turbine blade profiles. *Sakarya University Journal of Science* 22(5): 1432-1437

Figures

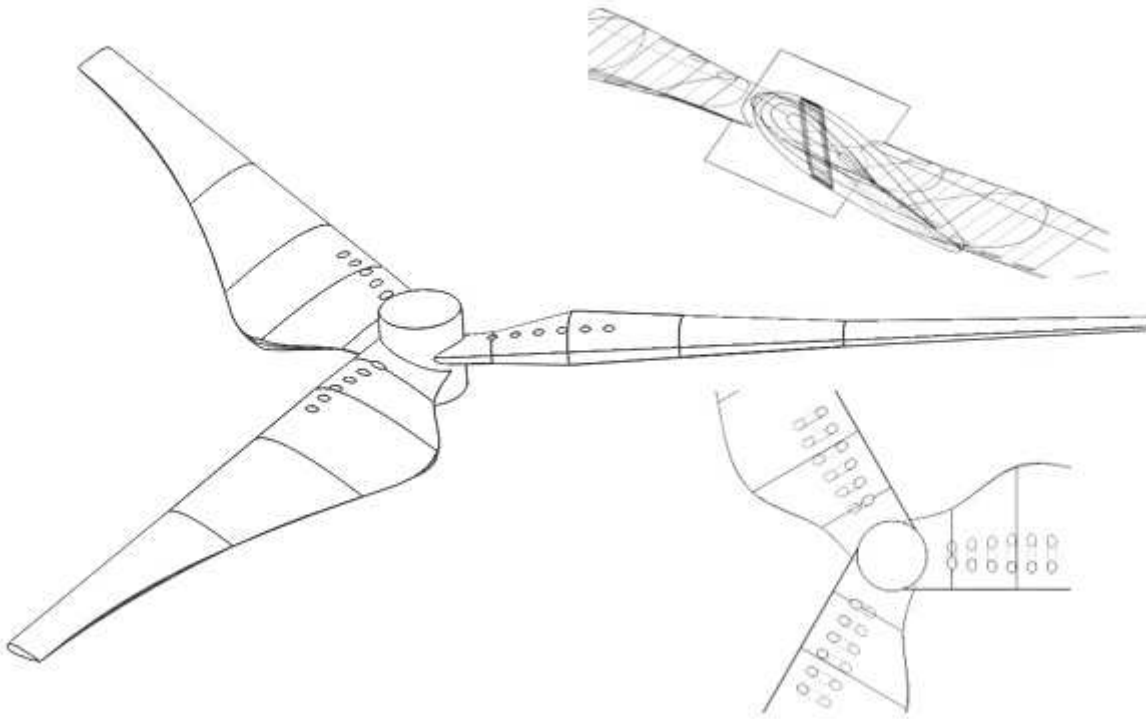


Figure 1

Horizontal-axis wind turbine with duct

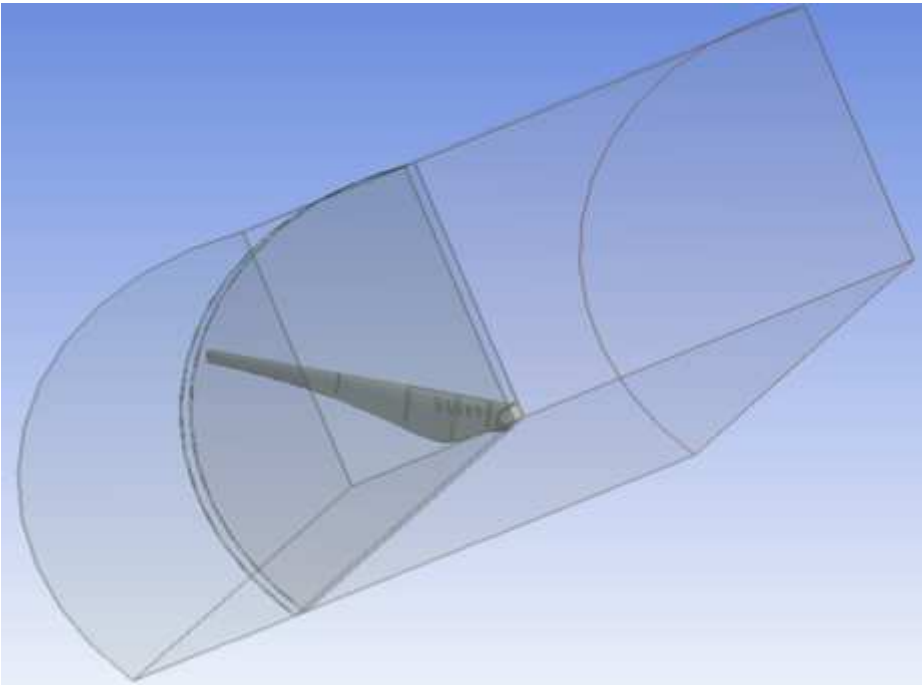


Figure 2

3D periodic calculation zone and boundary conditions

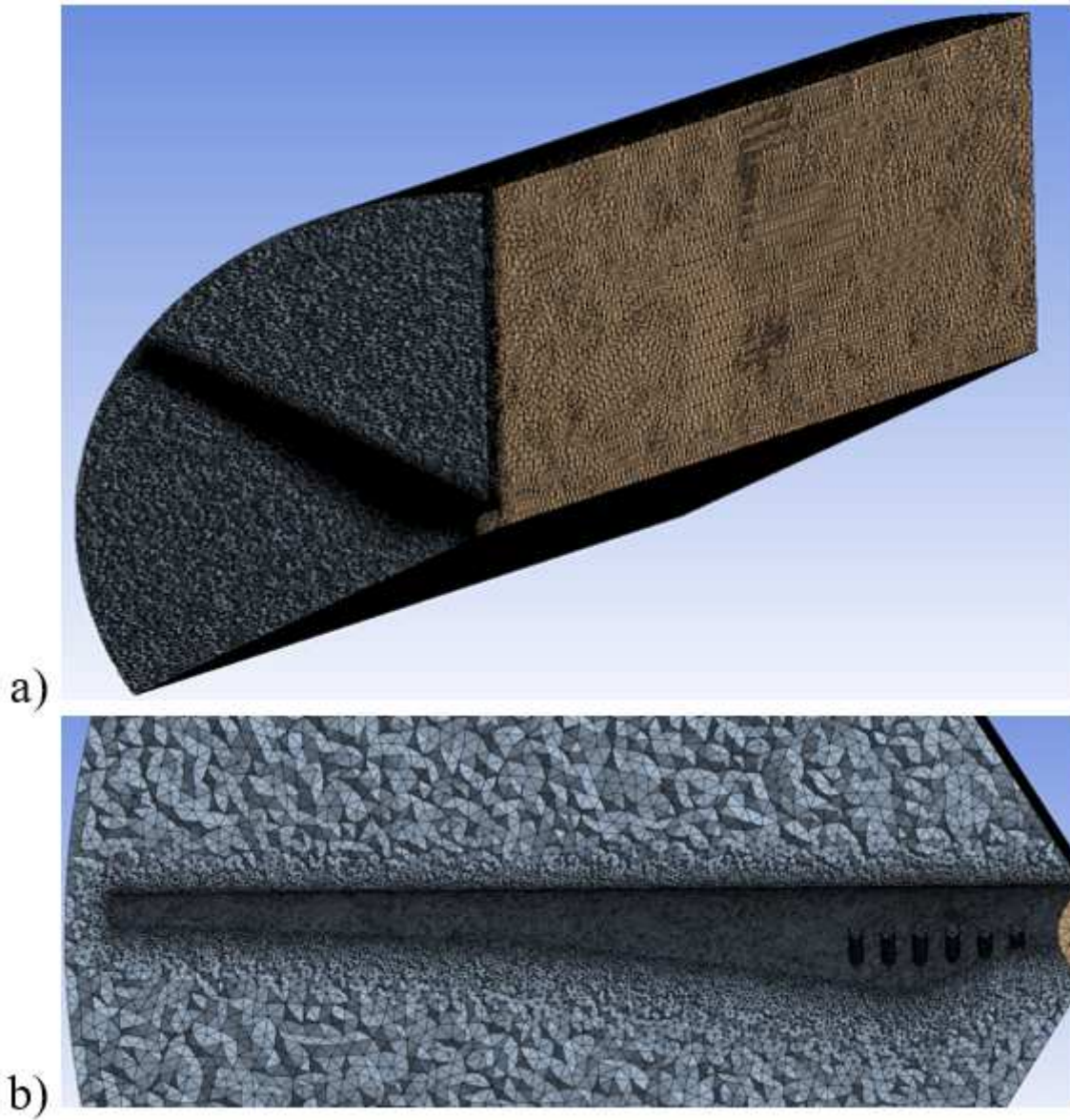


Figure 3

a) The mesh structure of the 3 model, b) The mesh structure around of the blade

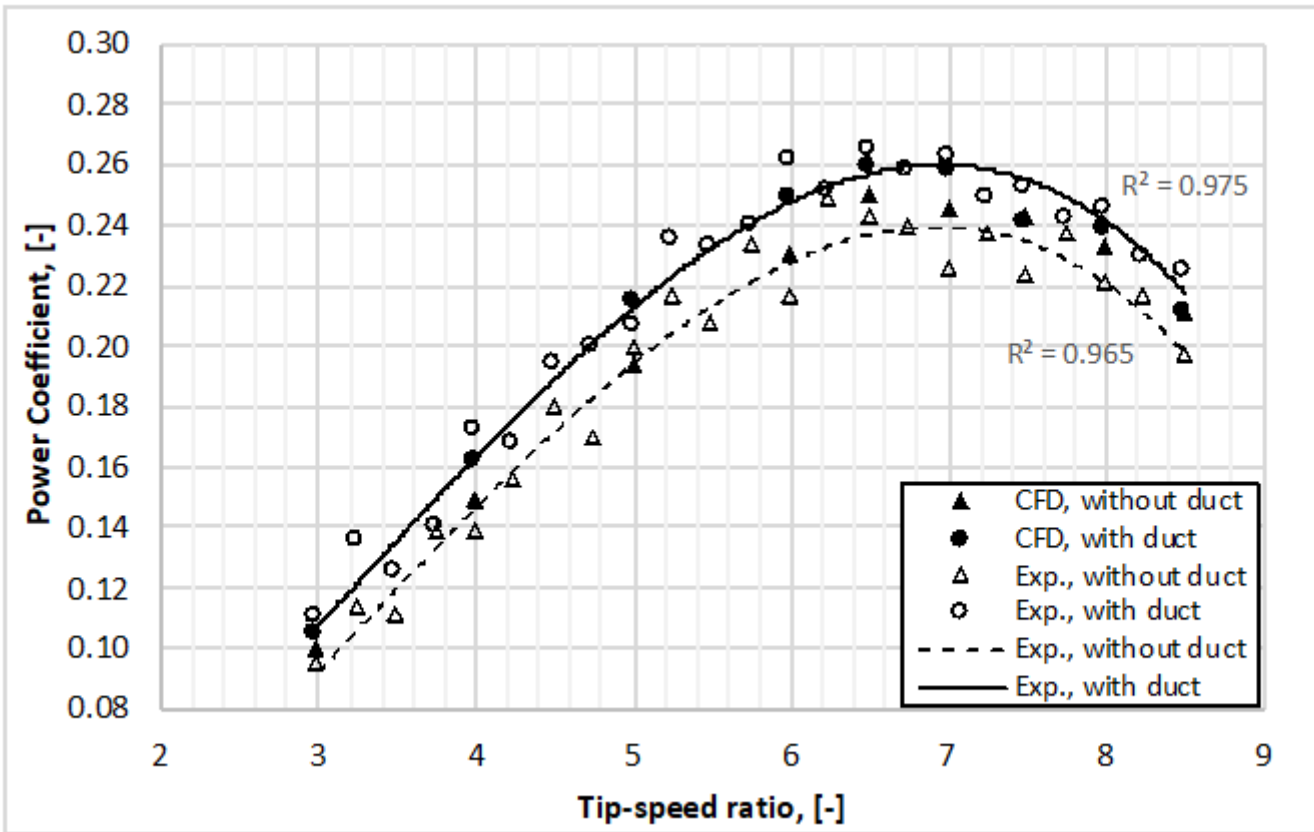


Figure 4

Comparison of the experimental study and CFD analysis results performed at 6 m/s air velocity and 7 tip-speed ratio

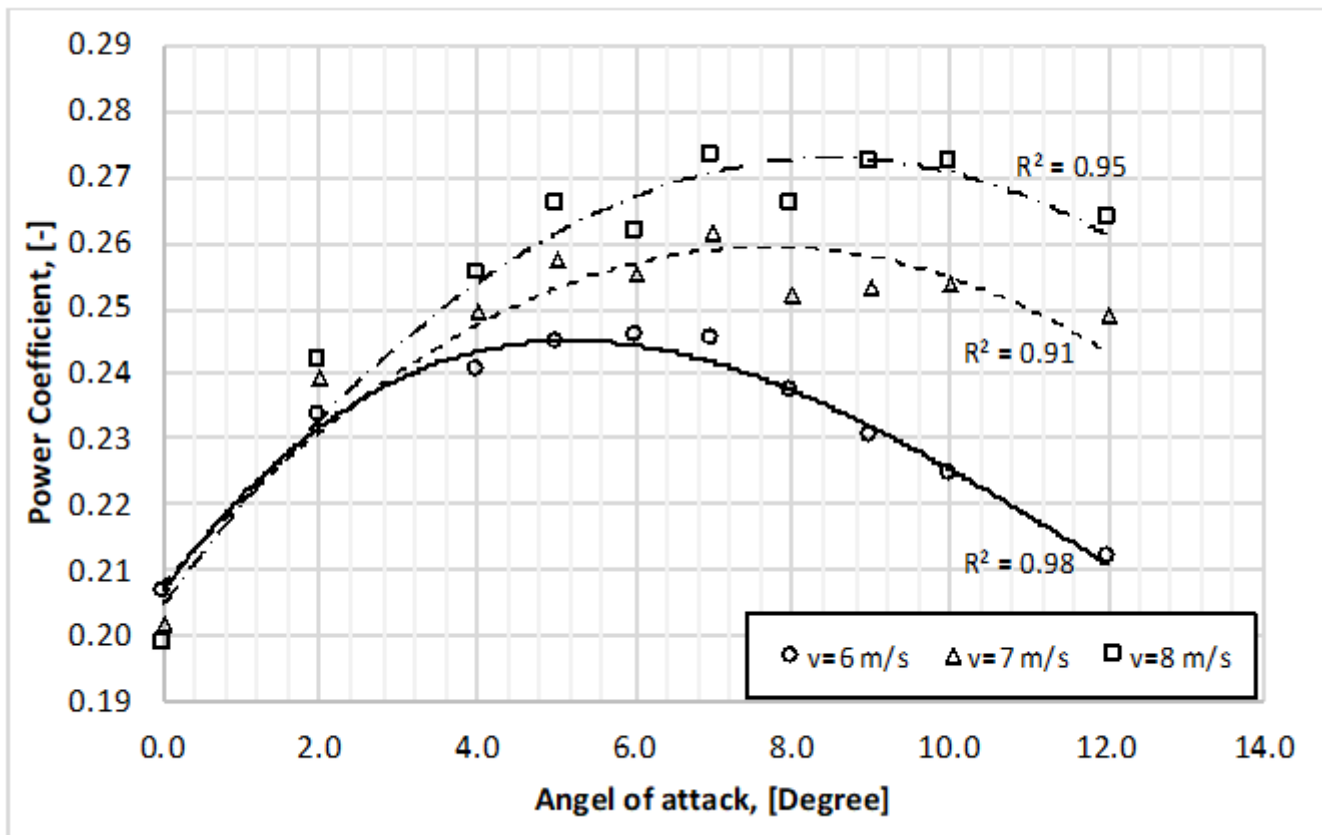


Figure 5

Power coefficient values based on the angle of attack at different airspeeds for air duct-free blade design

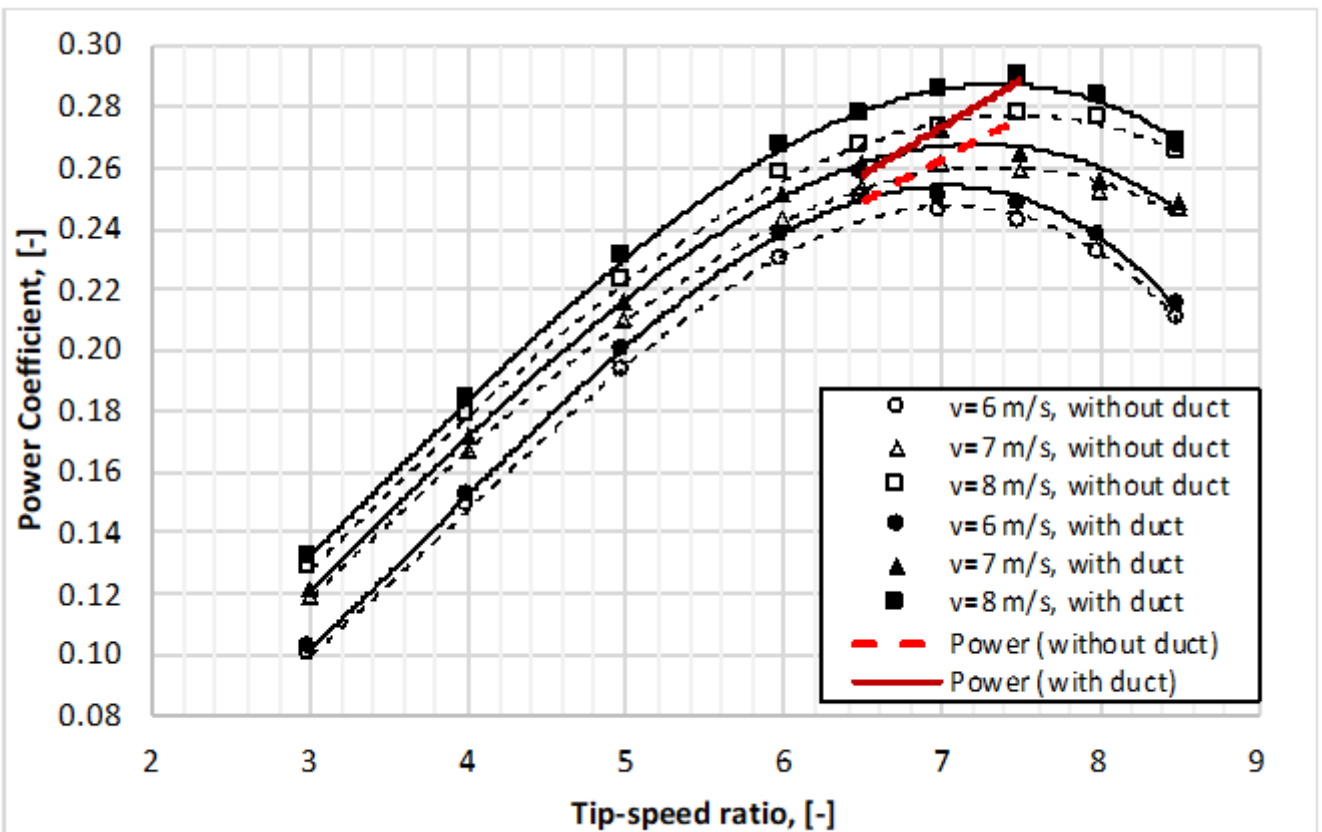
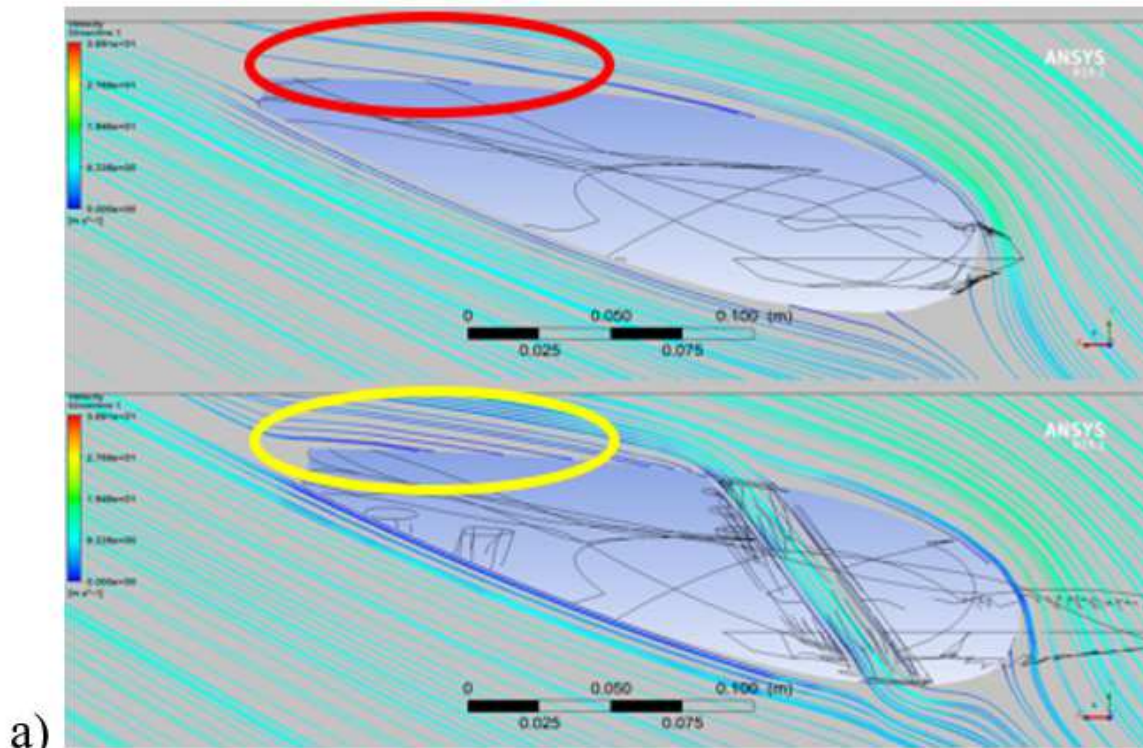
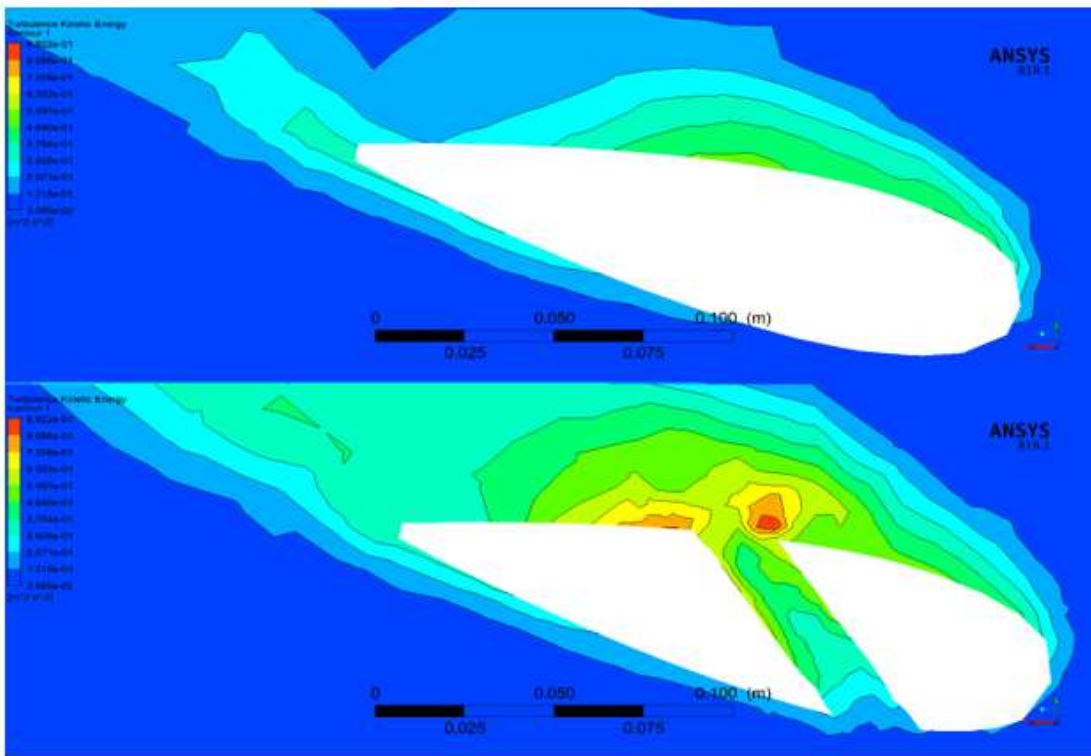


Figure 6

Power coefficients and maximum power curves obtained from the blade, which is designed with and without air ducts at various wind speeds, depending on the blade tip speed ratio



a)



b)

Figure 7

a) Streamlines in the blade profile section, b) Turbulence kinetic energy in the blade profile section

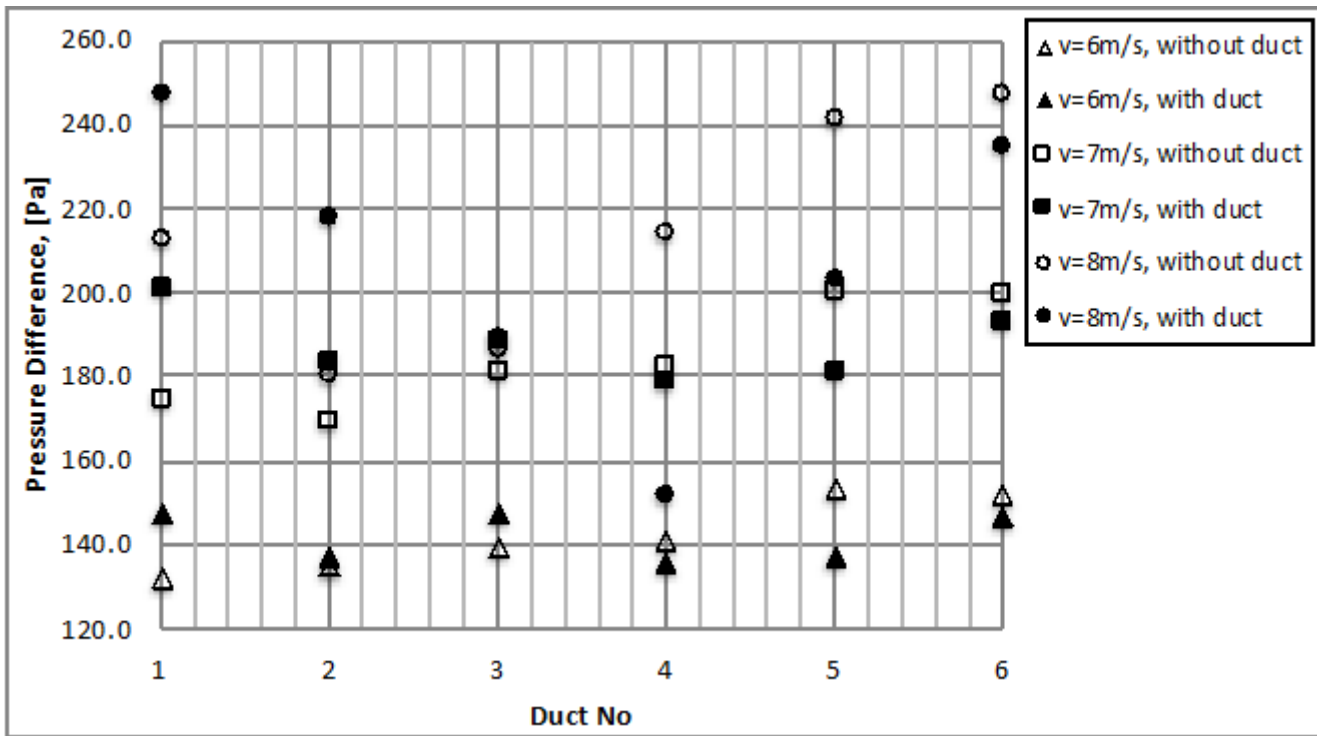


Figure 8

Maximum pressure differences on the plane passing through the centre of the air ducts